Environmental Science and Pollution Research (2023) 30:117132–117142
https://doi.org/10.1007/s11356-023-30468-x

RESEARCH ARTICLE

Synergistic effects of hydrogen peroxide and phosphate on uranium(VI) immobilization: implications for the remediation of groundwater at decommissioned in situ leaching uranium mine

Feng Li[1,2] · Xixian Huang[2] · Shasha Wang[2] · Hui Zhang[1,2] · Jianhong Ma[1,2] · Yang Ding[1,2] · Dexin Ding[1,2]

Received: 28 April 2023 / Accepted: 10 October 2023 / Published online: 21 October 2023

Abstract

The processes of acid in situ leaching (ISL) uranium (U) mines cause the pollution of groundwater. Phosphate (PO_4^{3-}) has the potential to immobilize U in groundwater through forming highly insoluble phosphate minerals, but the performance is highly restricted by low pH and high sulfate concentration. In this study, hydrogen peroxide (H_2O_2) and PO_4^{3-} were synergistically used for immobilizing U based on the specific properties of groundwater from a decommissioned acid ISL U mine. The removal mechanisms of U and the stability of U on the formed minerals were elucidated by employing X-ray diffraction, scanning electron microscopy, X-ray photoelectron spectroscopy and kinetic experiments. Our results indicated that the removal of U by simultaneously adding H_2O_2 and PO_4^{3-} was significantly higher than the removal of U by individually adding H_2O_2 or PO_4^{3-}. The removal of U increased with increasing PO_4^{3-} concentration from 20 to 200 mg L^{-1} while decreased with increasing H_2O_2 concentration from 0.003 to 0.3%. Specifically, the removal efficiency of U from groundwater reached 98% after the application of 0.003% H_2O_2 and 200 mg L^{-1} PO_4^{3-}. Amorphous iron phosphate that preferentially formed at low H_2O_2 and high PO_4^{3-} concentrations played a dominant role in U removal, while the formations of schwertmannite and crystalline iron phosphates may be also contributed to the removal of U. This was significantly different from the immobilization mechanism of U through the formation of uranyl phosphate minerals after adding phosphate. The kinetic experimental results suggested that the immobilized U had a good stability. Our research may provide a promising method for in situ remediating U-contaminated groundwater at the decommissioned acid ISL U mines.

Keywords Uranium · Immobilization · Hydrogen peroxide · Phosphate · Amorphous iron phosphate

Introduction

Acid in situ leaching (ISL) has been widely used for mining of sandstone-type of uranium (U) deposits (Mudd 2001a, b; Zhou et al. 2020). The process of acid ISL involves the injections of oxidant and leaching solution (e.g., sulfuric acid) into mineralized strata through injection wells, which can cause the rapid oxidation and dissolution of U (Ben Simon et al. 2014; Seredkin et al. 2016). Then U-bearing solutions are pumped out using production wells for further processing (Ben Simon et al. 2014). After decommissioning U mines, the residual U(VI) (e.g., several mg L^{-1}) will contaminate the groundwater (Taylor et al. 2004; Ding et al. 2015). The U-contaminated groundwater generally contains high SO_4^{2-} concentration and features with low pH due to the addition of leaching solution during the mining processes (Klimkova et al. 2011; Ding et al. 2015). Meanwhile, the groundwater at the decommissioned U mines is under anoxic conditions and contains high content of ferrous iron (Fe(II)) (Ram et al. 2011; Zhou et al. 2020). In most countries, remediation of the groundwater at decommissioned ISL U mines is required, and a series of remediation approaches, such as natural restoration, groundwater sweeping and forward

Responsible Editor: Georg Steinhauser

✉ Yang Ding
yding@usc.edu.cn

[1] Key Discipline Laboratory for National Defense for Biotechnology in Uranium Mining and Hydrometallurgy, University of South China, Hengyang 421001, People's Republic of China

[2] School of Resource & Environment and Safety Engineering, University of South China, Hengyang, Hunan 421001, People's Republic of China

recirculation, have been developed (Mudd 2001a; Borch et al. 2012; Saunders et al. 2016; Reimus et al. 2019). The natural restoration approach is dramatically restricted by hydro-geological conditions, while other approaches are costly since the U-contaminated groundwater need to be pumped out from the downstream wells and injected back to the upstream after the groundwater being treated (Fuller et al. 2002; Gallegos et al. 2015; Ruiz et al. 2019). Developing an economical and efficient method to remediate U-contaminated groundwater at decommissioned ISL U mines is essential for protecting environment and human health.

An alternative approach for pump-and-treat method is to manipulate the chemical or physical conditions of the groundwater to promote the formation of stable solid forms of U (Crane et al. 2011; Sharp et al. 2011; Ahmed et al. 2012), thus realizing in situ immobilization of U. The application of dissolved phosphate (PO_4^{3-}) or phosphate-containing minerals (e.g., hydroxyapatite) has been revealed to be useful for the remediation of U(VI)-contaminated groundwater through forming the precipitation of low solubility uranyl phosphate such as chernikovite ($H_3O(UO_2)(PO_4)\cdot 3H_2O$) and autunite ($Ca(UO_2)_2(PO_4)_2$) (Fuller et al. 2002; Mehta et al. 2015, 2016; Han et al. 2018). However, the precipitation of U with phosphate is highly limited at low pH and high sulfate concentration, due to the high dissolution rate of uranyl phosphate precipitation at low pH and the replacement of sulfate into the uranyl phosphate lattice at early stage of precipitation (Ohnuki et al. 2004; Fanizza et al. 2008). The reactive mineral surfaces can adsorb dissolved U(VI) and PO_4^{3-} to make the groundwater less saturated, which impedes the precipitation of uranyl phosphate, thus reducing the immobilization of U(VI) (Fuller et al. 2002; Singh et al. 2010; Mehta et al. 2015). Moreover, large excess of PO_4^{3-} was required to make a complete precipitation of U(VI) as uranyl phosphate compared with the amount of U(VI) (Fuller et al. 2002; Mehta et al. 2014; Foster et al. 2019), which may result in the secondary pollution of phosphorus. Previous study indicated that the formation of iron phosphate was a key mechanism for phosphorous removal in the Fe(II)/H_2O_2 oxidation system (Xing et al. 2021). Therefore, considering the high concentration of Fe(II) in groundwater at the decommissioned acid ISL U mines, it is reasonable to speculate that the simultaneous additions of H_2O_2 and PO_4^{3-} would facilitate the formations of iron phosphate minerals. The formed minerals could be used as adsorbents for the removal of U from groundwater, and concurrently reduce the residual PO_4^{3-} in groundwater. In addition, it has been revealed that H_2O_2 promoted the formation of schwertmannite under the conditions of high SO_4^{2-} and Fe(II) concentrations (Kumpulainen et al. 2008; Xie et al. 2017, 2022). Schwertmannite can remove contaminants through coprecipitation and sorption processes (Li et al. 2021; Ying et al. 2021). Overall, the collaborative use of H_2O_2 and PO_4^{3-} may be a promising method for immobilizing U in groundwater in situ.

The objective of this study was to propose a method by simultaneously using H_2O_2 and PO_4^{3-} for immobilizing U in groundwater at the decommissioned acid ISL U mine. Specifically, the effects of H_2O_2 and PO_4^{3-} concentrations on the removal of U from groundwater were to be investigated, and the optimum conditions were to be determined. The components, morphologies, elemental composition and chemical species of the formed solids were to be analyzed by a series of characterization methods. Based on the results of the removal experiments and the multiple characterizations of solids, the removal mechanisms of U in groundwater by adding H_2O_2 and PO_4^{3-} were to be elucidated. Moreover, the stability of the immobilized U was to be assessed by conducting the kinetic experiments of U release from the solids with a stirred-flow reactor. It was expected that the research would contribute to remediating U-contaminated groundwater at the decommissioned acid ISL U mine.

Materials and methods

Properties of groundwater from a decommissioned ISL U mine

The main chemical properties of the actual groundwater were determined based on our previous study (Ding et al. 2015). Briefly, the actual groundwater samples were collected from Northwest China. Acid ISL U mining technology was employed to exploit the sandstone U ore deposit in the mine. A large quantity of sulfuric acid solution was injected into the ore-bearing aquifer during the leaching processes. After the mine being decommissioned, the groundwater was contaminated by the residual SO_4^{2-} and U. The ore-bearing aquifer at the mine is in an anoxic condition based on the measured concentration of the dissolved oxygen (e.g., 0.3–0.5 mg L^{-1}). The concentration of Fe(II) in groundwater can reach several hundred milligrams per liter.

Experiments of U removal from groundwater

The simulated groundwater was prepared based on the main properties of the actual groundwater, including U (1000 μg L^{-1}), Fe(II) (300 mg L^{-1}) and SO_4^{2-} (2000 mg L^{-1}) concentrations, and pH value (3.0). After adding groundwater, H_2O_2 and PO_4^{3-} (K_2HPO_4) solutions were simultaneously added into the conical flasks. A series of initial H_2O_2 (0.003–0.3%) or PO_4^{3-} concentrations (20–200 mg L^{-1}) were used to investigate the effects of H_2O_2 or PO_4^{3-} concentration on U removal efficiency. We did not further add H_2O_2 and PO_4^{3-} during the reactions. The solution pH value

was recorded during the whole reactions. The suspension samples were collected, centrifuged at 3200 rpm and filtrated through 0.22 μm polyether sulfone filter (ANPEL, China). Note that, for the kinetic experiments with 0.003% H_2O_2 and 200 mg L^{-1} PO_4^{3-}, the suspension samples were obtained at specific sampling times (i.e., 0.5, 1, 2, 4, 8, 12 and 24 h) to determine the optimum reaction time. Then the concentration of U in the filtrates was analyzed using inductively coupled plasma mass spectrometry (ICP-MS) (Agilent 7700, Agilent Technologies, USA). The detection limit of U was 0.1 ppm, and the errors of the data were controlled within 10%. The resulting solid samples were freeze-dried, grounded, homogenized and then used for stirred-flow kinetic experiment. Meanwhile, the control experiments in which H_2O_2 or PO_4^{3-} was solely added were also conducted. The experiments were conducted in the anaerobic glove box, and the prepared groundwater, chemical reagent solution and deionized (DI) water were purged with Ar_2 to eliminate the interference of oxygen. All experiments were conducted at room temperature. The conditions of above experiments were presented in Table S1.

Characterizations of solid phase

Since the contents of U on solid samples collected from the removal experiments with U concentration of 1000 μg L^{-1} were lower than the detection limits of characterization instruments, we conducted another removal experiments with U concentration of 30 mg L^{-1}. The generated solid samples collected at 0.003% H_2O_2 and different PO_4^{3-} concentrations (e.g., 20, 50, 100 and 200 mg L^{-1}) and at 0.3% H_2O_2 and 200 mg L^{-1} PO_4^{3-} were characterized to explore the removal mechanisms of U from groundwater, using a combination of X-ray diffraction (XRD), Fourier transform infrared spectroscopy (FTIR), scanning electron microscopy (SEM) and X-ray photoelectron spectroscopy (XPS).

The crystal planes of the selected solid samples were analyzed with a TD-3500 X-ray diffractometer (XRD) (Tongda, China) to determine the main components of the mixed phases. The equipment was operated at 40 kV and 30 mA by step scanning from 10 to 70° 2θ at increments of 0.08° 2θ. FTIR was employed to detect the characteristic groups to further identify the composition of the solid phases. The mass ratio of sample to potassium bromide was 1:50. Each FTIR spectrum was recorded after 32 scans with 4 cm^{-1} resolution using a Nicolet iS10 spectrometer (ThermoFisher scientific, USA) with a deuterated triglycine sulfate (DTGS) detector. The spectra were then smoothed and baseline-corrected.

The surface morphologies of solid samples were characterized by SEM (Quanta 250, Bruker, Germany) equipped with energy dispersive spectroscope (EDS) detector. The samples were sputter-coated with carbon using an auto fine coater to enhance the electrical conductivity of samples. SEM-EDS was used to analyze the elemental composition. To characterize the chemical species of U and Fe- and S-containing groups, the samples were analyzed by XPS with a Thermo Fisher Scientific K-Alpha machine with an Al Kα X-ray source (1486.8 eV of photons) at 15 kV and 10 mA. Prior to individual elemental scans (i.e., Fe, O, U, S and P), a survey scan was taken for all the selected samples in order to detect the elements present. The Avantage software was used for data acquisition and analysis.

Kinetic experiments of U release

To evaluate the stability of U on the solid phases, the selected samples were used to conduct kinetic experiments in the short term using a stirred-flow reactor. The background electrolytes contained 2000 mg L^{-1} SO_4^{2-}, and the solution pH was 3.0. Before the kinetic experiments of U release, an aliquot of solid sample (i.e., 50 mg) and a magnetic stir bar were placed into the stirred-flow reactor (volume = 7.5 mL). The reactor was filled with background electrolyte. Then a filter membrane with a 25 mm diameter and 0.22 μm pore sizes was sealed on the reactor to prevent the outflow of solid particles. The suspension was stirred at 500 rpm, and the flow rate was set to 1 mL min^{-1} during the whole experiment. It should be noted that the flow rate and mixing rate can be well controlled to ensure a well-mixing of the diluted suspensions in the reactor and the continuous flow during the kinetic experiments (Tian et al. 2017; Wang et al. 2020). The background electrolyte solution was pumped through the reactor for 90 min release experiment, and the effluent solution was collected every 5 min. All effluent solution samples were acidified with concentrated HNO_3; the concentration of U in effluent solution was then analyzed using ICP-MS. All the release experiments were conducted at room temperature.

Results and discussion

Effects of H_2O_2 and PO_4^{3-} concentrations on U removal

Considering the low pH and high SO_4^{2-} and Fe(II) concentrations in U-contaminated groundwater at the decommissioned acid ISL U mine, a method for U removal by adding H_2O_2 and PO_4^{3-} was evaluated. Firstly, 0.003% and 200 mg L^{-1} PO_4^{3-} were chosen for conducting kinetic experiment, since the optimum removal efficiency of U was obtained at this condition. The results showed that the concentration of U in the supernatant after reactions quickly reached a plateau within 0.5 h (Fig. 1a). Thus, the reaction time was set to be 0.5 h for investigating the effects

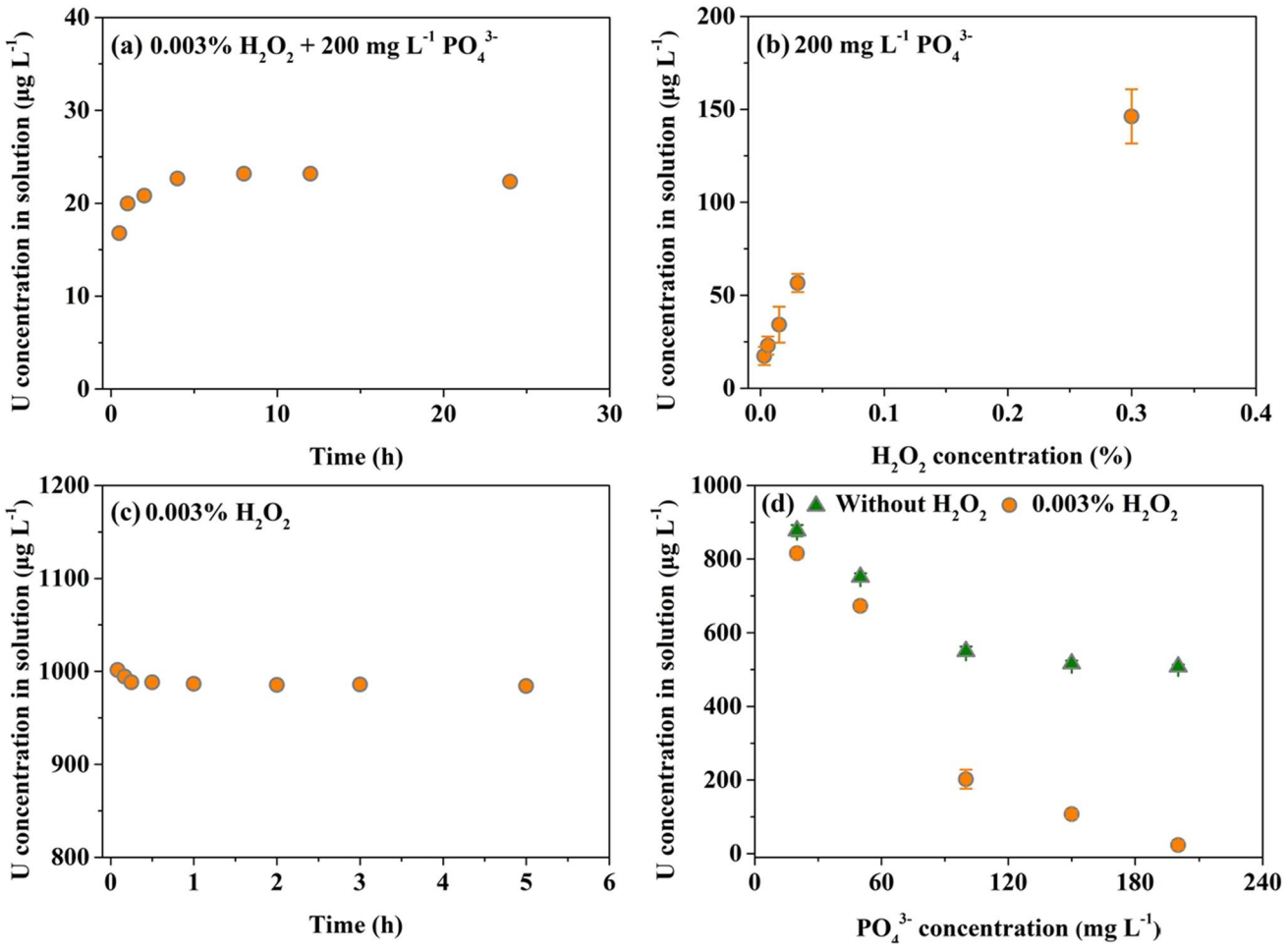

Fig. 1 **a** Kinetics of U removal from groundwater at 0.003% H_2O_2 and 200 mg L^{-1} PO_4^{3-}. **b** Effects of H_2O_2 concentrations on U removal at 200 mg L^{-1} PO_4^{3-}. **c** Kinetics of U removal from groundwater at 0.003% H_2O_2. **d** Effects of PO_4^{3-} concentrations on U removal at 0 and 0.003% H_2O_2. The reaction time for (**b**) and (**d**) was 0.5 h

of H_2O_2 or PO_4^{3-} concentration on the removal of U. As shown in Fig. 1b, the concentration of U in supernatant significantly increased with increasing H_2O_2 concentration when PO_4^{3-} concentration was 200 mg L^{-1}, indicating that a lower H_2O_2 concentration resulted in a higher removal of U. Without the addition of PO_4^{3-}, the concentration of U in supernatant slightly decreased with increasing reaction time at 0.003% H_2O_2 (Fig. 1c). Previous studies have demonstrated that the presence of H_2O_2 would facilitate the formation of schwertmannite, a poorly crystalline sulfate-containing Fe(III)-oxyhydroxy mineral, under the conditions of high concentrations of Fe(II) and SO_4^{2-} (Li et al. 2021; Xie et al. 2022). Schwertmannite has large amounts of reactive sites such as ≡Fe–O on its surface (Zhu et al. 2020; Li et al. 2021), which can react with UO_2^{2+}. However, a strong electrostatic repulsion between schwertmannite surface and UO_2^{2+} existed under our experimental conditions, since the point of zero charge of schwertmannite was at about neutral pH (Kumpulainen et al. 2008), leading to the low removal of U.

In the absence of H_2O_2, the concentration of U decreased from 877 to 550 μg L^{-1} with the increase of PO_4^{3-} concentration from 20 to 100 mg L^{-1} (Fig. 1d), which may be ascribed to the formation of insoluble PO_4-U phases (e.g., HUO_2PO_4). With further increasing PO_4^{3-} concentration, the concentration of U in supernatant showed no decrease. Nevertheless, the addition of H_2O_2 (0.003%) enhanced U removal especially at high PO_4^{3-} concentration (Fig. 1d). These results suggested that the combined effects of H_2O_2 and PO_4^{3-} mainly contributed to the removal of U from groundwater rather than the individual effect of H_2O_2 or PO_4^{3-}. Overall, the highest removal of U was found at 0.003% H_2O_2 and 200 mg L^{-1} PO_4^{3-}, and the residual U concentration in the treated groundwater was lower than the maximum contamination level of 30 μg L^{-1} prescribed by the World Health Organization (Ansoborlo et al. 2015) and

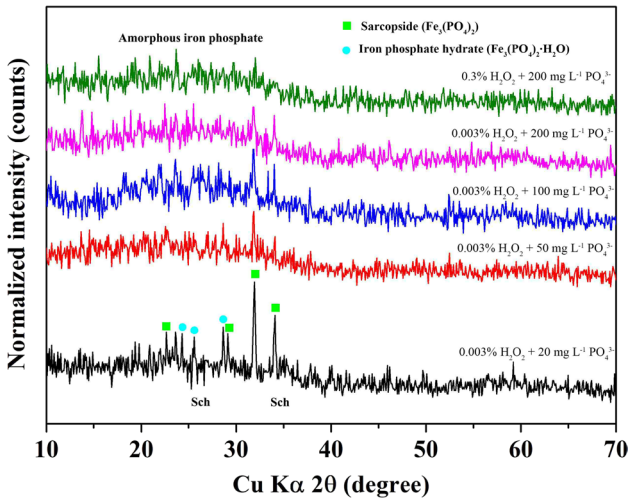

Fig. 2 X-ray diffraction (XRD) patterns of solid samples obtained at different H_2O_2 and PO_4^{3-} concentrations. The broad peak between 15° and 40° is attributed to the amorphous iron phosphate. Sch implies schwertmannite

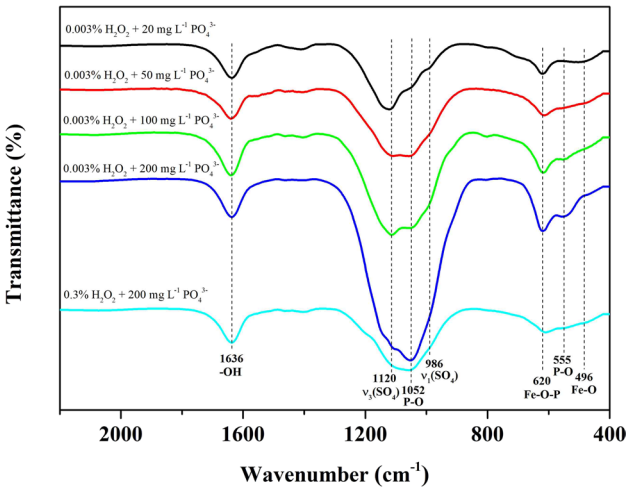

Fig. 3 Fourier transform infrared (FTIR) spectra of solid samples obtained at different H_2O_2 and PO_4^{3-} concentrations

United States Environmental Protection Agency, as well as lower than the background value of 60 μg L^{-1} from U mine.

Characterizations of the formed solids

To determine the components of the mixed solid phases, XRD patterns of the selected samples were analyzed. As depicted in Fig. 2, three main components were detected for solid sample obtained from the experimental condition of 0.003% H_2O_2 and 20 mg L^{-1} PO_4^{3-} according to PDF retrieval and previous studies (Bolloju et al. 2016; Zhang et al. 2019a), including crystalline sarcopside ($Fe_3(PO_4)_2$, ICSD#81-0695) and iron phosphate hydrate ($Fe_3(PO_4)_2{\cdot}H_2O$, ICSD#70-1794), and amorphous schwertmannite (JCPDS#47-1775). It is interesting to note that intensities of peaks referred to the crystalline iron phosphates significantly decreased with increasing PO_4^{3-} concentration from 20 to 200 mg L^{-1}, whereas a broad peak of amorphous iron phosphate (between 15° and 40°) obviously appeared (Palacios et al. 2012; Rudin and Pratsinis 2012). In addition, several peak signals of crystalline iron phosphates weakened when H_2O_2 concentration increased from 0.003 to 0.3%. XRD results suggested that different mechanisms may be responsible for U removal from groundwater when different concentrations of PO_4^{3-} were applied.

FTIR results further supported the formations of schwertmannite and iron phosphate minerals after the additions of H_2O_2 and PO_4^{3-} (Fig. 3). Specifically, the adsorption band at 986 cm^{-1} was attributed to a ν_1 fundamental of the symmetric SO_4^{2-} stretching, which resulted from SO_4^{2-} inner-sphere complexes (i.e., SO_4^{2-} in the tunnel structure of schwertmannite) (Blgham et al. 1990; Jönsson et al. 2005; Boily et al. 2010). The band at 1120 cm^{-1} was associated with the asymmetric SO_4^{2-} stretching (ν_3), corresponding to the adsorbed SO_4^{2-} (Boily et al. 2010; Wang et al. 2015). Meanwhile, the symmetric stretching and asymmetric bending vibrations of P–O bonds were observed at 1052 cm^{-1} and 555 cm^{-1}, respectively (Campos et al. 2021). The peak at 620 cm^{-1} was attributed to the stretching vibrations of Fe–O–P bonds in iron phosphate compounds (Liao et al. 2015). With the increase of PO_4^{3-} concentration, the relative intensities of SO_4^{2-} (ν_1 and ν_3) and Fe–O (496 cm^{-1}) vibration bands decreased, while the relative intensities of P–O and Fe–O–Fe bands increased. The results suggested that a higher PO_4^{3-} concentration may inhibit the formation of schwertmannite and facilitate the precipitation of iron phosphates, which was consistent with XRD results. In addition, intensities of the characteristic peaks of iron phosphates decreased with increasing H_2O_2 concentration from 0.003 to 0.3%, possibly due to the decreased formation of crystalline iron phosphates (XRD results) and the enhanced formation of schwertmannite at high H_2O_2 concentration.

For the solid samples obtained at 0.003% H_2O_2 and 20 mg L^{-1} PO_4^{3-}, substantial floccules coated on the aggregates (Fig. 4a). At lower PO_4^{3-} concentration (i.e., 20 mg L^{-1}), both schwertmannite (i.e., amorphous iron hydroxy sulfate mineral) and crystalline iron phosphates formed (see XRD results). With increasing PO_4^{3-} concentration from 20 to 100 mg L^{-1}, the aggregates became more compact (Fig. 4b, c), which may be attributed to the decreased formation of schwertmannite. However, the solid samples were dominated by flocculent aggregates with further increasing PO_4^{3-} concentration to 200 mg L^{-1} (Fig. 4d), which was ascribed to the considerably formed amorphous iron phosphate. These results suggested that different concentrations of PO_4^{3-} resulted in various morphologies and structures

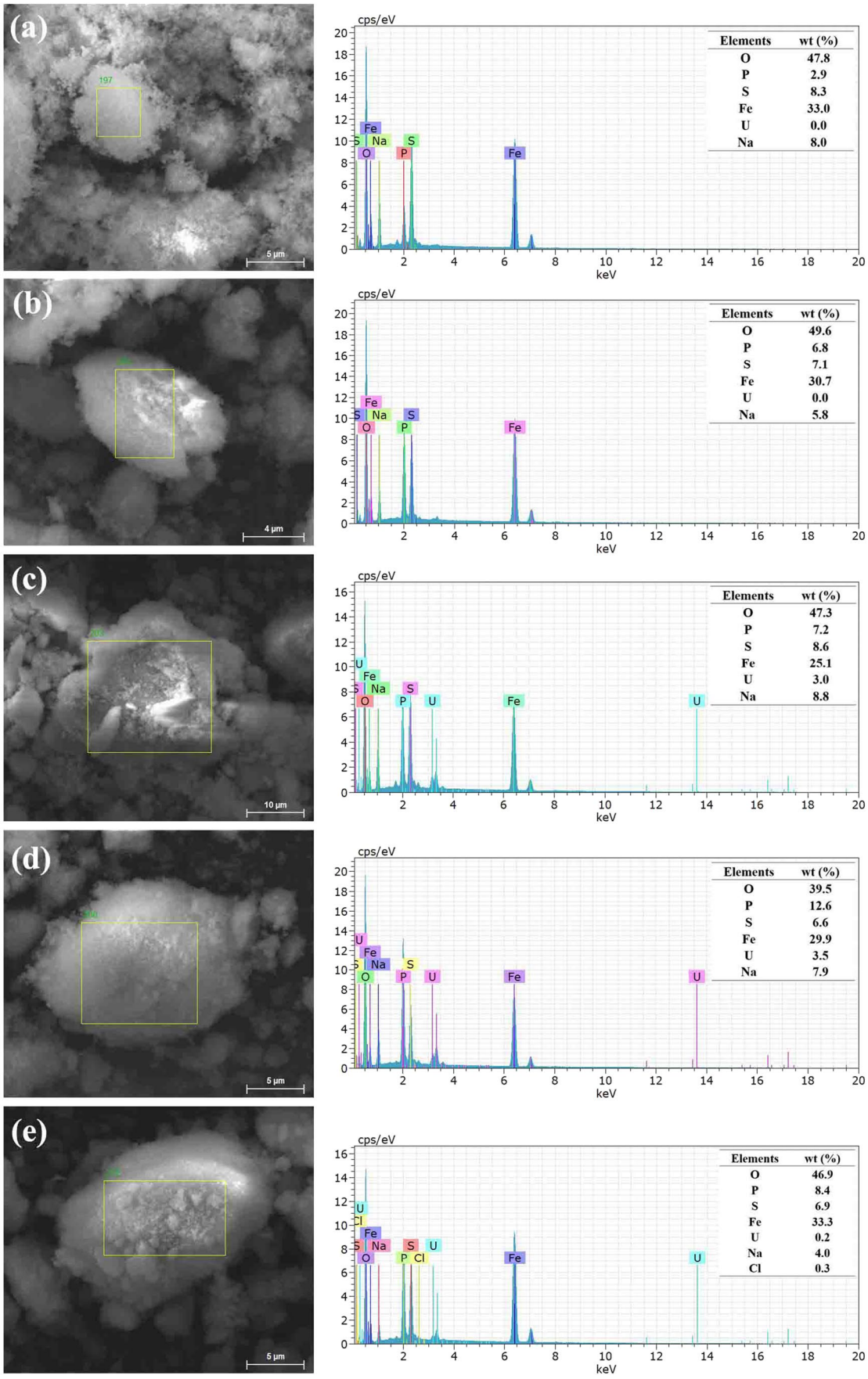
(a)
5 µm
cps/eV
keV
Elements wt (%)
O 47.8
P 2.9
S 8.3
Fe 33.0
U 0.0
Na 8.0
(b)
4 µm
cps/eV
keV
Elements wt (%)
O 49.6
P 6.8
S 7.1
Fe 30.7
U 0.0
Na 5.8
(c)
10 µm
cps/eV
keV
Elements wt (%)
O 47.3
P 7.2
S 8.6
Fe 25.1
U 3.0
Na 8.8
(d)
5 µm
cps/eV
keV
Elements wt (%)
O 39.5
P 12.6
S 6.6
Fe 29.9
U 3.5
Na 7.9
(e)
5 µm
cps/eV
keV
Elements wt (%)
O 46.9
P 8.4
S 6.9
Fe 33.3
U 0.2
Na 4.0
Cl 0.3

◂**Fig. 4** Scanning electron microscopy (SEM) EDS analysis for the elemental composition of solid samples obtained at **a** 0.003% H_2O_2 and 20 mg L^{-1} PO_4^{3-}, **b** 0.003% H_2O_2 and 50 mg L^{-1} PO_4^{3-}, **c** 0.003% H_2O_2 and 100 mg L^{-1} PO_4^{3-}, **d** 0.003% H_2O_2 and 200 mg L^{-1} PO_4^{3-} and (**e**) 0.3% H_2O_2 and 200 mg L^{-1} PO_4^{3-}

of the formed solids, which may affect the removal of U from groundwater. In this study, we did not find any significant effect of H_2O_2 concentration on the morphology and structure of the solids (Fig. 4 and Fig. S1). Furthermore, SEM-EDS was used to determine the elemental composition of the solids. Results showed that these aggregates mainly consisted of Fe, O, S, P and Na elements. When H_2O_2 concentration was 20 or 50 mg L^{-1}, the content of U on the aggregates was below the detection limit of EDS (Fig. 4a, b). The peaks of U were observed at 100 mg L^{-1} PO_4^{3-}, and the content of U accounted for 3.0% (wt%) (Fig. 4c). With the increase of PO_4^{3-} concentration from 100 to 200 mg L^{-1}, the content of U increased to 3.5% (wt%) (Fig. 4d). It appeared that the content of U on the aggregates correlated with P content. However, the increased H_2O_2 concentration (i.e., 0.3%) significantly reduced the content of U (0.2%) on the aggregates (Fig. 4e).

XPS analysis for Fe 2p, S2p and U 4f regions was conducted to quantify the chemical species of these elements on different solid samples. The Fe 2p core levels for all samples were split into 2p3/2 and 2p1/2 doublets (Fig. 5), and eight peaks were identified on the solids. Specifically, the peaks at 710.0, 711.3, 712.5 and 714.2 eV were attributed to Fe–O, Fe(OH)O, Fe–PO_4 and Fe–SO_4, respectively (Su et al. 2019; Zhang et al. 2019b). The relative abundance of Fe–PO_4 increased from 11.2 to 19.4%, while the relative abundances of Fe(OH)O and Fe–SO_4 decreased from 25.2 to 11.9% and from 19.5 to 17.2%, respectively, with increasing PO_4^{3-} concentration from 20 to 200 mg L^{-1}. This indicated that the content of iron phosphate minerals increased and the content of schwertmannite decreased in the solids with increasing PO_4^{3-} concentration, which further supported the analyses of XRD and FTIR. Results of U 4f spectra showed that U was present as U(VI) on all solid samples (Fig. S2). Moreover, the signal intensity of U significantly enhanced with increasing PO_4^{3-} concentration, suggesting that the increased PO_4^{3-} concentration facilitated the removal of U from groundwater.

Removal mechanisms of U from groundwater

Four processes could be involved in U removal by adding H_2O_2 and PO_4^{3-} based on the chemical experiments and solid characterizations. Results of XRD, FTIR and XPS analyses indicated that schwertmannite formed after adding H_2O_2 into the groundwater. The reactions can be expressed by the following equations:

$$2Fe^{2+}(aq) + H_2O_2(aq) + 2H^+(aq) = 2Fe^{3+}(aq) + 2H_2O(l) \quad (1)$$

$$8Fe^{3+}(aq) + (16 - 2x)H_2O(l) + xSO_4^{2-}(aq) = Fe_8O_8(OH)_{8-2x}(SO_4)_x(s)(sch) + (24 - 2x)H^+(aq) \quad (2)$$

where x gives normally a range between 1 and 1.75 (Li et al. 2021), and sch represents schwertmannite.

Schwertmannite can coprecipitate with UO_2^{2+} during its formation or sorb UO_2^{2+} through surface complexation. Due to the strong electrostatic repulsion between schwertmannite and UO_2^{2+} at low solution pH, the path way of U removal by schwertmannite was dramatically restricted, which was reflected by the slight decrease of U concentration in groundwater (from 1000 to 984 µg L^{-1}) after individually adding H_2O_2 (Fig. 1c). In addition, it has been revealed that the addition of PO_4^{3-} can remove U from acid mine drainages, laden process effluents and groundwaters, mainly through forming poorly soluble uranyl phosphate precipitates (Fuller et al. 2002; Singh et al. 2010; Kanematsu et al. 2014; Foster et al. 2019). In this study, although the concentration of U decreased from 1000 to 508 µg L^{-1} by individually adding PO_4^{3-} (200 mg L^{-1}) (Fig. 1d), the precipitation of U with PO_4^{3-} may not dominate the removal of U, since uranyl phosphate precipitates were not found by XRD, FTIR and XPS. A possible explanation was that other phosphate-containing precipitates (e.g., iron phosphates) preferentially formed in the presence of H_2O_2 compared with uranyl phosphate under our experimental conditions. The formation of reactive mineral (e.g., schwertmannite and iron phosphate minerals) can potentially limit the precipitation of uranyl phosphate by reducing the dissolved U(VI) and PO_4^{3-} to make the solution less saturated (Singh et al. 2010; Mehta et al. 2015).

It should be noted that the addition of H_2O_2 slightly enhanced U removal at 20 mg L^{-1} and 50 mg L^{-1} PO_4^{3-} (Fig. 1d), and the crystalline iron phosphate minerals (i.e., $Fe_3(PO_4)_2$ and $Fe_3(PO_4)_2{\cdot}H_2O$) mainly formed at low PO_4^{3-} concentration (Fig. 2) (Eq. 3). Therefore, the crystalline iron phosphate minerals should be also responsible for U removal possibly through surface sorption reaction, but the role of this process in U removal may be minor. Similar to schwertmannite, a strong electrostatic repulsion also existed between the surface of crystalline iron phosphate minerals and UO_2^{2+} at pH 3.0, since these crystalline minerals have relatively high point of zero charge (e.g., 5.3) (Thinnappan et al. 2008).

$$3Fe^{2+}(aq) + nH_2O + 2PO_4^{3-}(aq) = Fe_3\left(PO_4\right)_2 \cdot nH_2O(s) \quad (3)$$

When PO_4^{3-} concentration was higher than 50 mg L^{-1}, the addition of H_2O_2 dramatically enhanced U removal

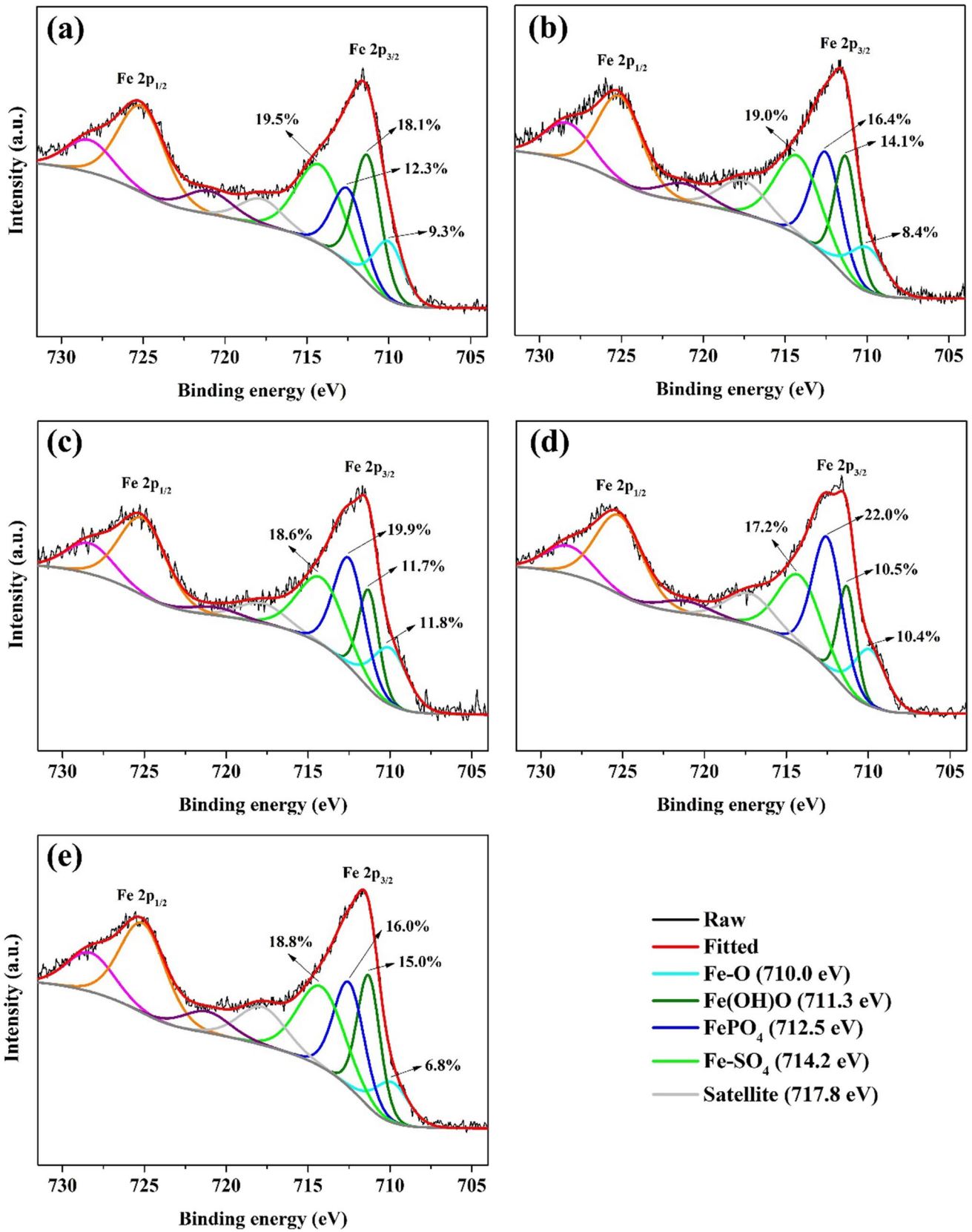

Fig. 5 X-ray photoelectron spectroscopy (XPS) Fe 2p region for solid samples obtained at **a** 0.003% H_2O_2 and 20 mg L^{-1} PO_4^{3-}, **b** 0.003% H_2O_2 and 50 mg L^{-1} PO_4^{3-}, **c** 0.003% H_2O_2 and 100 mg L^{-1} PO_4^{3-}, **d** 0.003% H_2O_2 and 200 mg L^{-1} PO_4^{3-} and **e** 0.3% H_2O_2 and 200 mg L^{-1} PO_4^{3-}

and facilitated the formation of amorphous iron phosphate (Figs. 1d and 2). The reactions can be described using Eqs. 1 and 4:

$$Fe^{3+}(aq) + PO_4^{3-}(aq) = FePO_4(s) \quad (4)$$

This agreed with previous finding that amorphous iron phosphate formed in the presence of high concentration of dissolved PO_4^{3-} via the oxidation of Fe(II) (Voegelin et al. 2010, 2013). Moreover, previous study has revealed that the point of zero charge of the amorphous iron phosphate was about 2.2 (Maarouf et al. 2021), which could promote the coprecipitation process of UO_2^{2+} during the formation of amorphous iron phosphate and the sorption of UO_2^{2+} on the amorphous iron phosphate surface. The sorption of UO_2^{2+} to amorphous iron phosphate surface mainly involves the binding of UO_2^{2+} to phosphoryl groups through corner sharing complexes, in which an equatorial oxygen atom of the UO_2^{2+} is shared with a PO_4^{3-} tetrahedron (Seder-Colomina et al. 2015), similar to uranyl-phosphate ternary complexes forming at the surface of iron (oxyhydr)oxides (e.g., goethite) upon UO_2^{2+} sorption in the presence of PO_4^{3-} (Singh et al. 2012). In addition, UO_2^{2+} can be sorbed and precipitated onto amorphous iron phosphate through the binding of UO_2^{2+} to FeO_6 octahedra to form bidentate surface complex and bidentate corner-sharing complexes (Rossberg et al. 2009; Singh et al. 2012; Seder-Colomina et al. 2015). It was thus reasonable to propose that most of U in groundwater was removed by amorphous iron phosphate through the coprecipitation and/or sorption.

Kinetics of U release from the solids

To assess the stability of the immobilized U, the selected solid samples were used to conduct the kinetic experiments. Fig. 6 showed that the effluent U concentration from solids obtained at 0.003% H_2O_2 quickly decreased within 60 min, and then was closely to zero. Specifically, at lower PO_4^{3-} concentrations (i.e., 20 and 50 mg L^{-1}), there was a similar release properties of U. In comparison, the release of U increased with increasing PO_4^{3-} concentration, which may be ascribed to the fact that the application of higher PO_4^{3-} concentrations immobilized more contents of U. It was obvious that the increased H_2O_2 concentration enhanced the release of U, possibly due to the decreased formation of amorphous iron phosphate at high H_2O_2 concentration (e.g., 0.3%). Furthermore, the total concentration of the released U from each solid sample was calculated after conducting the kinetic experiment. Results indicated that the total concentration of the released U from solid sample obtained at 0.003% H_2O_2 and 200 mg L^{-1} PO_4^{3-} was about 14 μg L^{-1}, which was far below the background concentration of U in groundwater at U mine. Overall, the kinetic experimental

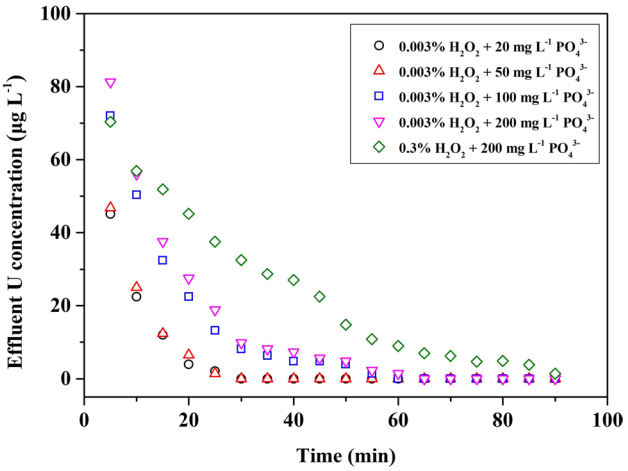

Fig. 6 Kinetics of U release from solid samples obtained at 0.003% H_2O_2 and 20–200 mg L^{-1} PO_4^{3-}, and 0.3% H_2O_2 and 200 mg L^{-1} PO_4^{3-}. The pH of background electrolytes was 3.0, and the release time was 90 min

results of U release may suggest that the immobilized U by adding H_2O_2 and PO_4^{3-} exhibited good stability at a short term, which was consistent with the static experimental results (Fig. 1a).

Conclusions

Due to the special properties of U-contaminated groundwater at acid ISL U mine (e.g., low pH and high concentrations of SO_4^{2-} and Fe(II)), the remediation of U-contaminated groundwater using the economical and efficient methods is still challenging. In this study, a method by simultaneously adding H_2O_2 and PO_4^{3-} was firstly applied to immobilize U(VI) in groundwater. Our results indicated that the removal of U from groundwater increased with increasing PO_4^{3-} concentration and decreased with increasing H_2O_2 concentration. Specifically, 0.003% H_2O_2 and 200 mg L^{-1} PO_4^{3-} were identified as the optimum conditions, which can reduce the residual U concentration to below 30 μg L^{-1}. Results of solid characterizations revealed that the formation of amorphous iron phosphate at low H_2O_2 concentration and high PO_4^{3-} concentration was mainly responsible for the removal of U, possibly through coprecipitation and sorption processes. The formed schwertmannite and crystalline iron phosphates may also participate in the removal of U. Furthermore, the immobilized U by the formed minerals showed a good stability based on the kinetic experimental results. In addition, the proposed method can significantly reduce the residual PO_4^{3-} in groundwater, which was ascribed to the formation of crystalline and amorphous iron phosphate minerals. The stability of the immobilized U was assessed within several hours in this study. However, the changes of

groundwater properties and hydrological conditions may affect the sequestration of U on the formed solids. Thus, it is desired to evaluate the long-term stability of the immobilized U (e.g., several months to years) under condition variations (e.g., pH and background ion concentrations) to test the feasibility of this method. Overall, our results may provide a promising method for in situ immobilization of U in groundwater at the decommissioned acid ISL U mines.

Supplementary Information The online version contains supplementary material available at https://doi.org/10.1007/s11356-023-30468-x.

Author contributions This study was conceptualized by Y.D. Data collection and analysis were performed by F. L. and Y.D. The experiments were conducted by S.S.W. The first draft of the manuscript was written by F.L. The reviewing and editing of the manuscript were performed by X.X.H., H.Z., J.H.M., Y.D. and D.X.D. The final version of the manuscript has been read and approved by all authors.

Funding This study was supported by the National Natural Science Foundation of China (42207309, U1967210), the Natural Science Foundation of Hunan Province (2022JJ40369) and the University of South China Innovation Foundation (X202210555234).

Data availability Data and materials can be made available upon request.

Declarations

Ethics approval and consent to participate Not applicable.

Consent for publication Not applicable.

Competing interests The authors declare no competing interests.

References

Ahmed B, Cao B, Mishra B, Boyanov MI, Kemner KM, Fredrickson JK, Beyenal H (2012) Immobilization of U(VI) from oxic groundwater by Hanford 300 Area sediments and effects of Columbia River water. Water Res 46:3989–3998

Ansoborlo E, Lebaron-Jacobs L, Prat O (2015) Uranium in drinking-water: a unique case of guideline value increases and discrepancies between chemical and radiochemical guidelines. Environ Int 77:1–4

Ben Simon R, Thiry M, Schmitt JM, Lagneau V, Langlais V, Bélières M (2014) Kinetic reactive transport modelling of column tests for uranium In Situ Recovery (ISR) mining. Appl Geochem 51:116–129

Blgham JM, Schwertmann U, Carlson L, Murad E (1990) A poorly crystallized oxyhydroxysulfate of iron formed by bacterial oxidation of Fe(II) in acid mine waters. Geochim Cosmochim Acta 54:2743–2758

Boily JF, Gassman PL, Peretyazhko T, Szanyi J, Zachara JM (2010) FTIR spectral components of schwertmannite. Environ Sci Technol 44:1185–1190

Bolloju S, Rohan R, Wu ST, Yen HX, Dwivedi GD, Lin YA, Lee JT (2016) A green and facile approach for hydrothermal synthesis of $LiFePO_4$ using iron metal directly. Electrochim Acta 220:164–168

Borch T, Roche N, Johnson TE (2012) Determination of contaminant levels and remediation efficacy in groundwater at a former in situ recovery uranium mine. J Environ Monit 14:1814–1823

Campos PV, Albuquerque ARL, Angélica RS, Paz SPA (2021) FTIR spectral signatures of amazon inorganic phosphates: igneous, weathering, and biogenetic origin. Spectrochim Acta A 251:119476

Crane RA, Dickinson M, Popescu IC, Scott TB (2011) Magnetite and zero-valent iron nanoparticles for the remediation of uranium contaminated environmental water. Water Res 45:2931–2942

Ding DX, Li SM, Hu N, Xu F, Li GY, Wang YD (2015) Bioreduction of U(VI) in groundwater under anoxic conditions from a decommissioned in situ leaching uranium mine. Bioprocess Biosyst Eng 38:661–669

Fanizza MF, Yoon H, Zhang C, Oostrom M, Wietsma TW, Hess NJ, Bowden ME, Strathmann TJ, Finneran KT, Werth CJ (2008) Porescale evaluation of uranyl phosphate precipitation in a model groundwater system. Water Resour Res 49:874–890

Foster RI, Kim KW, Oh MK, Lee KY (2019) Effective removal of uranium via phosphate addition for the treatment of uranium laden process effluents. Water Res 158:82–93

Fuller CC, Bargar JR, Davis JA, Piana MJ (2002) Mechanisms of uranium interactions with hydroxyapatite: implications for groundwater remediation. Environ Sci Technol 36:158–165

Gallegos TJ, Campbell KM, Zielinski RA, Reimus PW, Clay JT, Janot N, Bargar JR, Benzel WM (2015) Persistent U(IV) and U(VI) following in-situ recovery (ISR) mining of a sandstone uranium deposit, Wyoming, USA. Appl Geochem 63:222–234

Han M, Kong L, Hu X, Chen D, Xiong X, Zhang H, Su M, Diao Z, Ruan Y (2018) Phase migration and transformation of uranium in mineralized immobilization by wasted bio-hydroxyapatite. J Clean Prod 197:886–894

Jönsson J, Persson P, Sjöberg S, Lövgren L (2005) Schwertmannite precipitated from acid mine drainage: phase transformation, sulphate release and surface properties. Appl Geochem 20:179–191

Kanematsu M, Perdrial N, Um W, Chorover J, O'Day PA (2014) Influence of phosphate and silica on U(VI) precipitation from acidic and neutralized wastewaters. Environ Sci Technol 48:6097–6106

Klimkova S, Cernik M, Lacinova L, Filip J, Jancik D, Zboril R (2011) Zero-valent iron nanoparticles in treatment of acid mine water from in situ uranium leaching. Chemosphere 82:1178–1184

Kumpulainen S, von der Kammer F, Hofmann T (2008) Humic acid adsorption and surface charge effects on schwertmannite and goethite in acid sulphate waters. Water Res 42:2051–2060

Li X, Guo C, Jin X, He C, Yao Q, Lu G, Dang Z (2021) Mechanisms of Cr(VI) adsorption on schwertmannite under environmental disturbance: changes in surface complex structures. J Hazard Mater 416:125781

Liao Q, Wang F, Chen PS, Zhu H, Lu M, Qin J (2015) FTIR spectra and properties of iron borophosphate glasses containing simulated nuclear wastes. J Mol Struct 1092:187–191

Maarouf F, Saoiabi S, Azzaoui K, Chrika C, Khalil H, Elkaouni S, Lhimr S, Boubker O, Hammouti B, Jodeh S (2021) Statistical optimization of amorphous iron phosphate: inorganic sol–gel synthesis-sodium potential insertion. BMC Chem 15:1–14

Mehta VS, Maillot F, Wang Z, Catalano JG, Giammar DE (2014) Effect of co-solutes on the products and solubility of uranium(VI) precipitated with phosphate. Chem Geol 364:66–75

Mehta VS, Maillot F, Wang Z, Catalano JG, Giammar DE (2015) Transport of U(VI) through sediments amended with phosphate to induce in situ uranium immobilization. Water Res 69:307–317

Mehta VS, Maillot F, Wang Z, Catalano JG, Giammar DE (2016) Effect of reaction pathway on the extent and mechanism of Uranium(VI) immobilization with calcium and phosphate. Environ Sci Technol 50:3128–3136

Mudd GM (2001a) Critical review of acid in situ leach uranium mining: 1. USA and Australia Environ Geol 41:390–403

Mudd GM (2001b) Critical review of acid in situ leach uranium mining: 2. Soviet Block and Asia Environ Geol 41:404–416

Ohnuki T, Kozai N, Samadfam M, Yasuda R, Yamamoto S, Narumi K, Naramoto H, Murakami T (2004) The formation of autunite ($Ca(UO_2)_2(PO_4)_2{\cdot}nH_2O$) within the leached layer of dissolving apatite: incorporation mechanism of uranium by apatite. Chem Geol 211:1–14

Palacios E, Leret P, Fernández JF, De Aza AH, Rodríguez MA (2012) Synthesis of amorphous acid iron phosphate nanoparticles. J Nanopart Res 14:1131

Ram R, Charalambous F, Tardio J, Bhargava S (2011) An investigation on the effects of Fe (FeIII, FeII) and oxidation reduction potential on the dissolution of synthetic uraninite (UO_2). Hydrometallurgy 109:125–130

Reimus PW, Dangelmayr MA, Clay JT, Chamberlain KR (2019) Uranium natural attenuation downgradient of an in situ recovery mine inferred from a cross-hole field test. Environ Sci Technol 53:7483–7493

Rossberg A, Ulrich KU, Weiss S, Tsushima S, Hiemstra T, Scheinostt AC (2009) Identification of uranyl surface complexes on ferrihydrite: Advanced EXAFS data analysis and CD-MUSIC modeling. Environ Sci Technol 43:1400–1406

Rudin T, Pratsinis SE (2012) Homogeneous iron phosphate nanoparticles by combustion of sprays. Ind Eng Chem Res 51:7891–7900

Ruiz O, Thomson B, Cerrato JM, Rodriguez-Freire L (2019) Groundwater restoration following in-situ recovery (ISR) mining of uranium. Appl Geochem 109:104418

Saunders JA, Pivetz BE, Voorhies N, Wilkin RT (2016) Potential aquifer vulnerability in regions down-gradient from uranium in situ recovery (ISR) sites. J Environ Manage 183:67–83

Seder-Colomina M, Morin G, Brest J, Ona-Nguema G, Gordien N, Pernelle JJ, Banerjee D, Mathon O, Esposito G, van Hullebusch ED (2015) Uranium (VI) scavenging by amorphous iron phosphate encrusting Sphaerotilus natans filaments. Environ Sci Technol 49:14065–14075

Seredkin M, Zabolotsky A, Jeffress G (2016) In situ recovery, an alternative to conventional methods of mining: exploration, resource estimation, environmental issues, project evaluation and economics. Ore Geol Rev 79:500–514

Sharp JO, Lezama-Pacheco JS, Schofield EJ, Junier P, Ulrich KU, Chinni S, Veeramani H, Margot-Roquier C, Webb SM, Tebo BM, Giammar DE, Bargar JR, Bernier-Latmani R (2011) Uranium speciation and stability after reductive immobilization in aquifer sediments. Geochim Cosmochim Acta 75:6497–6510

Singh A, Catalano JG, Ulrich KU, Giammar DE (2012) Molecular-scale structure of uranium(VI) immobilized with goethite and phosphate. Environ Sci Technol 46:6594–6603

Singh A, Ulrich KU, Giammar DE (2010) Impact of phosphate on U(VI) immobilization in the presence of goethite. Geochim Cosmochim Acta 74:6324–6343

Su X, Li X, Ma L, Fan J (2019) Formation and transformation of schwertmannite in the classic Fenton process. J Environ Sci 82:145–154

Taylor G, Farrington V, Woods P, Ring R, Molloy R (2004) Review of environmental impacts of the acid in situ leach uranium mining process. In: CSIRO Land and Water Client Report. CSIRO, Clayton, Victoria, p 60

Thinnappan V, Merrifield CM, Islam FS, Polya DA, Wincott P, Wogelius RA (2008) A combined experimental study of vivianite and As (V) reactivity in the pH range 2–11. Appl Geochem 23:3187–3204

Tian L, Shi Z, Lu Y, Dohnalkova AC, Lin Z, Dang Z (2017) Kinetics of cation and oxyanion adsorption and desorption on ferrihydrite: roles of ferrihydrite binding sites and a unified model. Environ Sci Technol 51:10605–10614

Voegelin A, Kaegi R, Frommer J, Vantelon D, Hug SJ (2010) Effect of phosphate, silicate, and Ca on Fe(III)-precipitates formed in aerated Fe(II)- and As(III)-containing water studied by X-ray absorption spectroscopy. Geochim Cosmochim Acta 74:164–186

Voegelin A, Senn AC, Kaegi R, Hug SJ, Mangold S (2013) Dynamic Fe-precipitate formation induced by Fe(II) oxidation in aerated phosphate-containing water. Geochim Cosmochim Acta 117:216–231

Wang P, Lu Y, Hu S, Tian L, Liang Y, Shi Z (2020) Kinetics of Ni reaction with organic matter-ferrihydrite composites: experiments and modeling. Chem Eng J 379:122306

Wang X, Gu C, Feng X, Zhu M (2015) Sulfate local coordination environment in schwertmannite. Environ Sci Technol 49:10440–10448

Xie Y, Lu G, Ye H, Yang C, Xia D, Yi X, Reinfelder J, Dang Z (2017) Fulvic acid induced the liberation of chromium from CrO_4^{2-}-substituted schwertmannite. Chem Geol 475:52–61

Xie Y, Ye H, Wen Z, Dang Z, Lu G (2022) Sulfide-induced repartition of chromium associated with schwertmannite in acid mine drainage: impacts and mechanisms. Sci Total Environ 848:157863

Xing C, Shi J, Cui F, Shen J, Li H (2021) Fe^{2+}/H_2O_2-Strengite method with the enhanced settlement for phosphorus removal and recovery from pharmaceutical effluents. Chemosphere 277:130343

Ying H, Huang K, Feng X, Yan Y, Zhu M, Wang Z, Huang Q, Wang X (2021) As(III) adsorption–oxidation behavior and mechanisms on Cr(VI)-incorporated schwertmannite. Environ Sci Nano 8:1593–1602

Zhang B, Wang L, Li Y (2019b) Fractionation and identification of iron-phosphorus compounds in sewage sludge. Chemosphere 223:250–256

Zhang Z, Guo G, Li X, Zhao Q, Bi X, Wu K, Chen H (2019a) Effects of hydrogen-peroxide supply rate on schwertmannite microstructure and chromium(VI) adsorption performance. J Hazard Mater 367:520–528

Zhou Y, Li G, Xu L, Liu J, Sun Z, Shi W (2020) Uranium recovery from sandstone-type uranium deposit by acid in-situ leaching—an example from the Kujieertai. Hydrometallurgy 191:105209

Zhu J, Chen F, Gan M (2020) Controllable biosynthesis of nanoscale schwertmannite and the application in heavy metal effective removal. Appl Surf Sci 529:147012